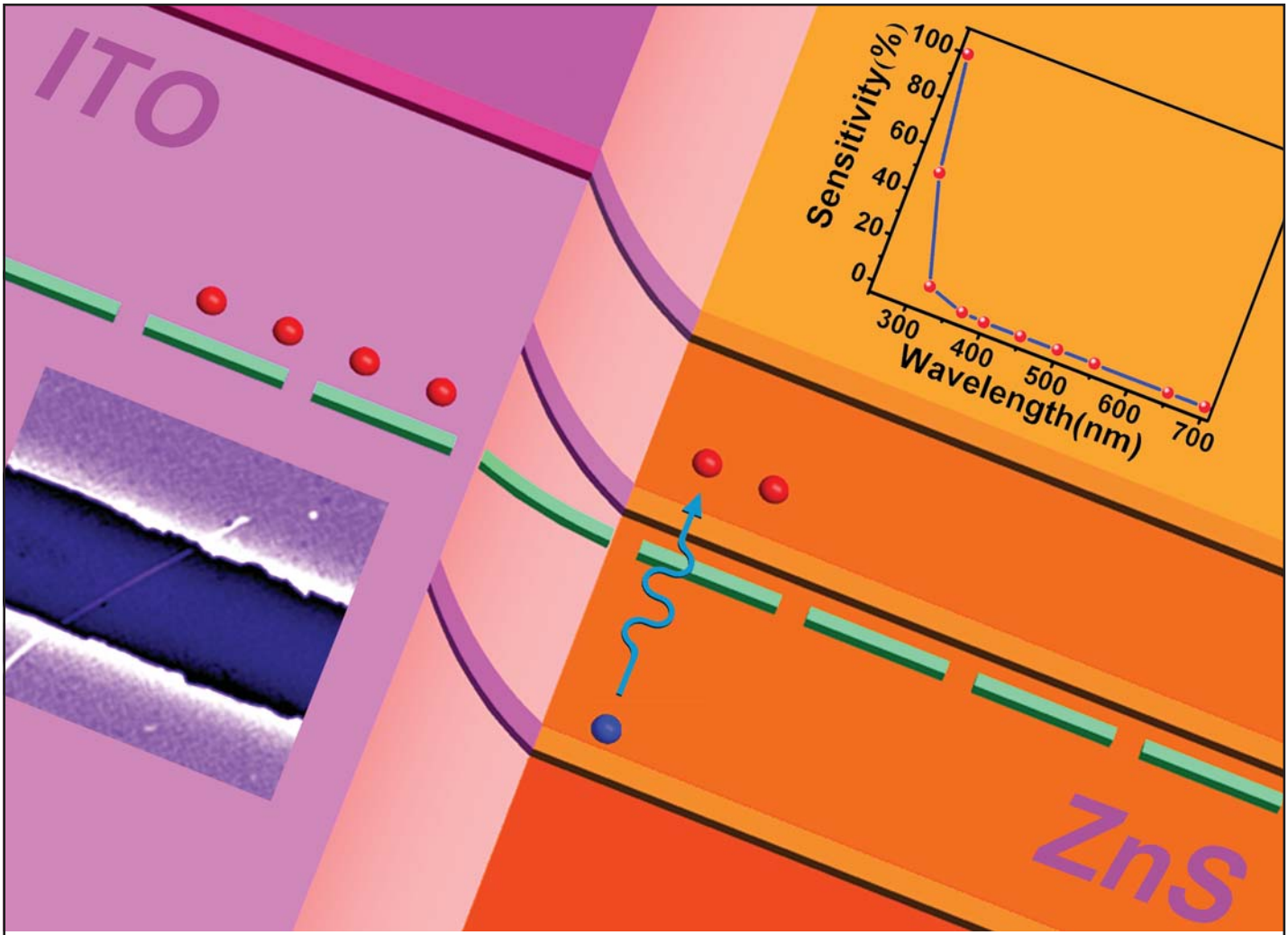

Showcasing research from Professor Jiansheng Jie's Micro/Nano Functional Materials and Devices Lab in the School of Electronic Science and Applied Physics, Hefei University of Technology, China.

Title: High-gain visible-blind UV photodetectors based on chlorine-doped n-type ZnS nanoribbons with tunable optoelectronic properties

By tuning the optoelectronic properties *via* chloride doping and using ITO as the ohmic contact, ZnS nanoribbon visible-light blind UV photodetectors show extremely high photoconductive gain. These high gain ZnS nano-photodetectors have great developmental potential for weak light detection with detection limitation down to a single photon.

As featured in:

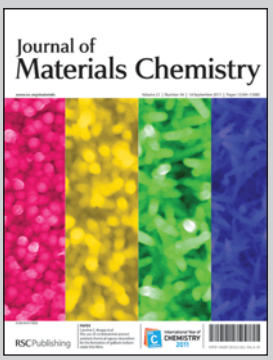

See Yongqiang Yu *et al.*, *J. Mater. Chem.*, 2011, **21**, 12632.

RSC Publishing

www.rsc.org/materials

Registered Charity Number 207890

Journal of Materials Chemistry

Dynamic Article Links

Cite this: J. Mater. Chem., 2011, 21, 12632

www.rsc.org/materials

PAPER

High-gain visible-blind UV photodetectors based on chlorine-doped n-type ZnS nanoribbons with tunable optoelectronic properties†

Yongqiang Yu,[ab] Jiansheng Jie,*[a] Peng Jiang,[a] Li Wang,[a] Chunyan Wu,[a] Qiang Peng,[a] Xiwei Zhang,[a] Zhi Wang,[a] Chao Xie,[a] Di Wu[b] and Yang Jiang*[b]

Received 4th April 2011, Accepted 17th May 2011
DOI: 10.1039/c1jm11408e

Efficient n-type doping of ZnS nanoribbons (NRs) were accomplished by using chlorine (Cl) as the dopant *via* thermal evaporation. An indium tin oxide (ITO) transparent electrode was used to achieve ohmic contact to the ZnS:Cl NRs. The conductivity of the Cl-doped ZnS NRs was significantly improved as compared with the undoped ones and could be tuned to a wide range of 3–4 orders of magnitude by adjusting the Cl doping level. High-performance nano-photodetectors were constructed based on the ZnS:Cl NRs, which show high sensitivity to the UV light while are nearly blind to the visible light. Notably, the ZnS:Cl NR photodetectors have a photoconductive gain as high as $\sim 10^7$, which is amongst the highest values obtained for UV nano-photodetectors so far. Our results demonstrate that the n-type ZnS NRs with tunable optoelectronic properties are promising building blocks for nano-optoelectronic devices.

1 Introduction

Zinc sulfide (ZnS), an important II–VI compound semiconductor with a wide direct bandgap of 3.7 eV, has applications in diverse fields such as flat panel displays,[1] light-emitting diodes (LEDs),[2] and injection lasers.[3] Recently, ZnS nanostructures have attracted increasing attention due to their potential application in a new generation of nano-electronics and nano-optoelectronics.[4] Intrinsic or unintentionally doped ZnS nanostructures are highly insulating due to the high crystal quality with little donor/acceptor defects and are thus not suitable for device applications. The ability to control the optoelectronic properties of ZnS nanostructures *via* doping is essential in order to realize the future applications. Current research on ZnS nanostructures is mainly focused on the material growth and structure and characterization of optical properties. Studies on their transport properties are rare. Although various metal elements including Mn, Cu, Fe, Co, and Eu have been used as dopants to modulate the optical and magnetic properties of ZnS nanostructures,[5–10] reliable and reproducible doping remains a big challenge. Research on n- and p-type doping of ZnS nanostructures is less than critical and still at the very early stage.[11,12]

The development of visible-blind, UV photodetectors is of great importance for optoelectronic and environmental applications. ZnS nanostructures are promising materials for high-performance UV photodetectors owing to the wide bandgap in the UV regime, high quantum-efficiency, high crystallinity, and potential advantages in quantum confinement and size effects. Although nanoscale UV photodetectors based on a variety of wide band-gap nanomaterials such as ZnO and GaN nanowires (NWs) have been investigated,[13,14] ZnS nano-photodetectors are rarely studied and reported.[15,16] This situation might be the result of the difficulties in controlling the transport properties of ZnS nanostructures as well as obtaining good contact between the semiconductor and the electrode.

Herein, we report on the tuning of the electronic and optoelectronic properties of n-type ZnS nanoribbons (NRs) *via* chloride (Cl) doping. Cl was selected as the n-type dopant since it has been reported to be an efficient dopant for achieving high levels of n-type doping with less defects in n-ZnS film.[17,18] Excellent ohmic contact can also be achieved by replacing conventional metallic electrodes with transparent, conducting indium tin oxide (ITO) electrodes. Near visible-blind UV nano-photodetectors with extremely high photoconductive gain ($\sim 10^7$) were also demonstrated based on the n-type ZnS:Cl NRs.

2 Experimental details

2.1 ZnS:Cl NRs synthesis and characterization

ZnS:Cl NRs were synthesized in a horizontal quartz tube furnace by using a thermal co-evaporation method.[9] 0.3 g ZnS power (99.99%, Aldrich) was first loaded into an alumina boat and then

[a]*School of Electronic Science and Applied Physics, Hefei University of Technology, Hefei, Anhui, 230009, P. R. China. E-mail: jason.jsjie@gmail.com*
[b]*School of Materials Science and Engineering, Hefei University of Technology, Hefei, Anhui, 230009, P. R. China. E-mail: apjiang@hfut.edu.cn*

† Electronic supplementary information (ESI) available. See DOI: 10.1039/c1jm11408e

the boat was transferred to the center region of the furnace. Si substrates coated with 5 nm gold were placed at a distance of ~10 cm downstream from the ZnS source. Another boat filled with $ZnCl_2$ powder was used as the Cl dopant source and placed at a distance of 12 cm upstream from the ZnS source. The system was then evacuated to a base pressure of 4×10^{-5} Torr, and backfilled with a constant H_2 (5% in Ar) gas flow of 40 sccm to a pressure of ~150 Torr. The ZnS source was heated up to 1060 °C in one hour and kept at that temperature for 60 min. Three samples with varied chloride doping levels were synthesized, labeled as sample 1, sample 2, and sample 3, corresponding to the molar ratio of $ZnCl_2$: ZnS changed from 1 : 4 to 1 : 2 and 1 : 1 in experiments, respectively. Undoped ZnS NRs were also synthesized under the same conditions except $ZnCl_2$ was not used for comparison.

Morphologies and structures of the as-synthesized ZnS:Cl NRs were characterized by X-ray diffraction (XRD, Rigaku D/Max-rB), field-emission scanning electron microscopy (FE-SEM, SIRION 200 FEG) and high-resolution transmission electron microscopy (HRTEM, Philips CM200 FEG). Compositions of the ZnS:Cl NRs were analyzed by X-ray photoelectron spectroscopy (XPS, Thermo ESCALAB 250). Room-temperature photoluminescence (RT-PL, LabRAM-HR) spectra were obtained by using He–Cd 325 nm laser as the excitation source.

2.2 Device construction

In order to construct the field-effect transistors (FETs) based on a single ZnS NR, the NRs were first dispersed on a SiO_2 (300 nm)/p^+-Si substrate and then ITO (100 nm) electrodes were deposited on individual NRs using a pulsed laser deposition (PLD) system with KrF excimer laser (Lambda Physik COMPexPro 102, 248 nm, 120 mJ, 5 Hz) and a shadow mask that consisted of 5 μm thick tungsten wires. Various metallic electrodes such as Ti, In, Ag, Al, and Au were also deposited by a high-vacuum electron-beam (EB) evaporation system for comparison. Post-annealing at 500 °C for 10 min at vacuum (4×10^{-5} Torr) was carried out to further improve the electrical contact of ITO with ZnS:Cl NRs.

2.3 Device characterization

The electrical transport characteristics of the ZnS:Cl NRs were measured using a Keithley 4200 semiconductor characterization system. To detect the photoconductive properties of ZnS:Cl NRs, monochromatic light from a source composed of a xenon lamp (150 W) and a monochromator (Omni-λ300) was focused and guided onto the NRs perpendicularly. The light was turned ON and OFF manually to investigate the time response of the ZnS:Cl NR photodetectors.

3 Results and discussions

3.1 Characterization of the n-type ZnS:Cl NRs

A typical SEM image of the as-synthesized ZnS:Cl NRs indicates that the NRs have width in the range of 50–500 nm, length of 20–100 μm, and thickness of 10–50 nm (Fig. 1a). The sizes are uniform along the NR length. The inset in Fig. 1a depicts the energy-dispersive X-ray spectroscopy (EDX) profile of sample 2,

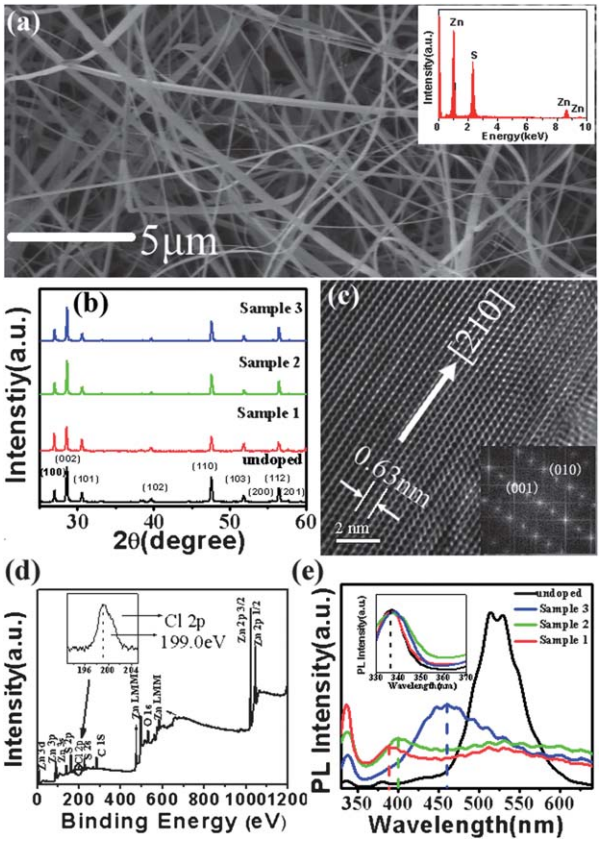

Fig. 1 (a) A typical SEM image of ZnS:Cl NRs from sample 2. The inset is the corresponding EDX spectrum. (b) XRD patterns of both undoped and Cl-doped ZnS NRs. (c) HRTEM image of the ZnS:Cl NR. The inset shows the corresponding FFT pattern. (d) XPS spectra of ZnS:Cl NRs (for sample 2). The inset shows the enlarged Cl 2p peak. (e) PL spectra of both undoped and Cl-doped ZnS NRs. The inset shows the enlarged band-edge emission peaks of the samples, which are normalized for comparison.

revealing a near stoichiometric ratio of Zn : S ≈ 50 : 49. XRD patterns of the ZnS:Cl NR samples (1–3), together with the undoped sample for comparison, are shown in Fig. 1b. All the diffraction peaks in the patterns can be properly assigned to ZnS with a wurtzite structure and no impurity phases are detected, suggesting the high phase purity of the products. In addition, no obvious peak shift is observed for the ZnS:Cl NRs in relation to the undoped ZnS NR. This can be attributed to the similar ionic radius of Cl^- (1.81 Å) with S^{2-} (1.84 Å). From a typical HRTEM image and corresponding fast Fourier transform (FFT) pattern (Fig. 1c), it can be concluded that ZnS:Cl NRs have a wurtzite single-crystal structure with a growth direction of [210]. Further XPS investigation reveals the presence of Cl in the sample (Fig. 1d). XPS measurements of all of the samples indicate an increasing atomic ratio of Cl in the samples from 2% for sample 1 to 3% for sample 2, and 4% for sample 3. However, no Cl signal is detected in the undoped sample, implying that efficient Cl doping is achieved in the ZnS:Cl NRs.

Fig. 1e depicts the RT-PL spectra of both the undoped and doped ZnS NRs. Four emission peaks can be observed from the undoped ZnS NRs, which correspond to the near-band edge (NBE) emission at 335 nm, and emissions associated with the

zinc vacancies (380 nm), zinc interstitials (436 nm), and sulfur vacancies (530 nm), respectively.[19] As for the ZnS:Cl NRs, the emissions from zinc defects diminished, while a new emission peak located at 390–460 nm emerged. This new emission peak could be ascribed to the self-activated (SA) luminescence that corresponds to the donor–acceptor pair (DAP) transition from the isolated Cl donor level to the acceptor level of the SA centers consisting of zinc vacancies (V_{Zn}) and substitutional Cl ions associated at one of the nearest sites.[17] In particular, the emission at 456 nm for sample 3 is in good agreement with the SA luminescence observed in ZnS:Cl thin films.[19] The observation of SA luminescence confirms that most of the Cl atoms introduced by Cl doping have successfully entered into the sulfur sites in the ZnS NRs.[17,20] On the other hand, when the Cl doping concentration is increased, the SA emission peak shifts to a longer wavelength, along with the increase of peak intensity, due to the increase of the acceptor level. The change in the SA emission peak could also be regarded as indirect evidence for the achievement of controlled Cl doping in the ZnS NRs. The regular red-shift of the SA emission from 380 nm to ~525 nm also reveals that the optical properties of the NRs could be tuned by simply adjusting the doping level.

3.2 Ohmic contact to the n-type ZnS:Cl NRs

In order to determine the effects of Cl doping on the transport properties of ZnS NRs, electrical measurements were conducted by constructing nano-FETs based on individual ZnS:Cl NRs. Attempts to achieve ohmic contact with the ZnS:Cl NRs by using various metallic electrodes, including Ti, In, Ag, Al, and Au, as the source–drain electrodes, all failed. Contact resistance was so high that only very low conduction current could be detected for the ZnS:Cl NR devices (Fig. 2a). Fortunately, ITO was found to be able to provide much better contact with the ZnS:Cl NRs than conventional metallic electrodes. Fig. 2a clearly shows that the conduction current was substantially improved when ITO was used as the electrode. The transport characteristics of the ZnS:Cl NRs with varied doping concentrations were measured using ITO electrodes (Fig. 2b). The linear I–V curves indicate the good ohmic contact of ITO with the ZnS:Cl NRs. Significantly, we note that the conductance of the ZnS NRs increases remarkably with the increasing of Cl dopant. The undoped ZnS NRs are highly insulating (conductivity < 10^{-8} S cm^{-1}), while the ZnS:Cl NRs exhibit much enhanced conductivity of 7.5×10^{-3} S cm^{-1}, 0.25 S cm^{-1} and 5.0 S cm^{-1} for sample 1, sample 2, and sample 3, respectively. The conductivity distribution of 15 NR samples is shown in Fig. 2c. It is clear that the conductivity of the ZnS NRs can be tuned to a wide range of at least three orders of magnitude by adjusting the Cl^- doping level. Moreover, the conductivity of ZnS:Cl NRs can be remarkably improved by 1–2 orders of magnitude after a post-annealing process at 500 °C for 10 min (Fig. 2d), which is likely to be attributed to the further reduction of the contact resistance.

Although ohmic contact is essential for high-performance electronic and optoelectronic devices, it should be noted that Schottky contact has been achieved with metallic electrodes such as Ag,[12] Cr,[15] Au,[21] and Pt:Ga[22] in nanodevices based on n-ZnS and n-ZnSe nanostructures. The contact problem remains to be the main barrier for the development of useful applications for

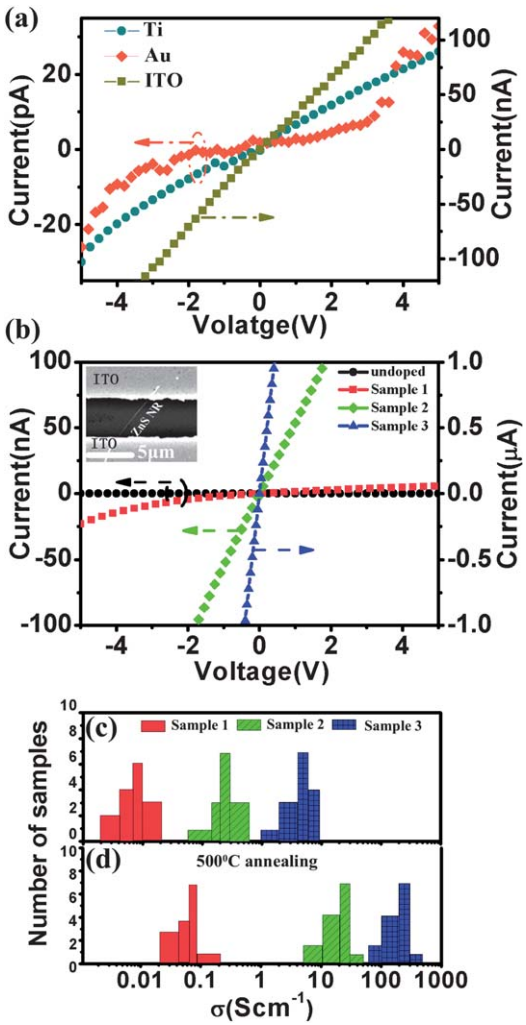

Fig. 2 (a) Typical I–V curves of a single ZnS:Cl NR (sample 2) measured using different kinds of source–drain electrodes. (b) Typical I–V curves of undoped ZnS NR and Cl-doped NRs with increased doping concentration from sample 1 to sample 3. The inset shows a typical SEM image of the nano-FET fabricated from an individual ZnS:Cl NR. (c) Distribution of conductivity values for 45 devices, 15 devices each for sample 1, sample 2, and sample 3. (d) Conductivity distribution of the devices after annealing.

ZnS nanostructures. The surface Fermi level pinning induced by the surface states has been suggested to be responsible for the non-ohmic contact behavior (Fig. 3). The high density surface states such as defects and dangling bonds on the ZnS surface will lead to the Fermi level pinning at φ_0. φ_0 represents the energy level that below which all the surface states must be filled for charge neutrality at the surface. Due to the negatively charged surface resulting from acceptor states, the surface energy band will bend upwards and thus form a large contact barrier at the interface. A previous study using photoelectric yield measurement revealed a surface barrier (qV_D) as high as 1.2 eV at the ZnS surface.[23] Therefore, a large contact barrier will always exist at the metal/semiconductor interface, no matter what kind of metallic electrode is used. For ZnS films, the barrier heights are estimated to be about 1.5 eV and 0.8 eV for In and Al, respectively, and even higher for Ag and Au.[24] In contrast, the surface

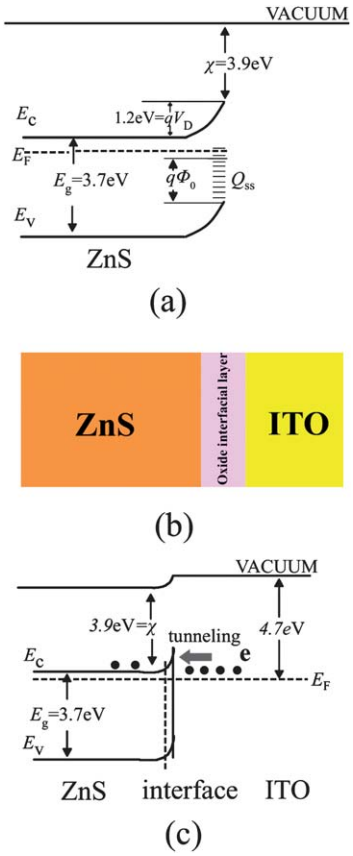

Fig. 3 (a) Energy-band diagram illustrating the Fermi energy level pinning at the n-ZnS surface. (b) Schematic illustration of the ITO/n-ZnS contact. An oxide interfacial layer is expected to generate at the interface. (c) Equilibrium band diagram schematic for ITO/n-ZnS (E_c the conduction-band edge, E_v the valence-band edge, E_F the Fermi level, Q_{ss} the surface-state density on ZnS).

states are likely to be saturated by the ITO layer, thus avoiding the surface Fermi level pinning. Moreover, a highly conductive interfacial oxide layer is likely to be formed at the interface by surface reactions between ZnS and ITO during the PLD process, where the surface of ZnS was oxidized and some indium atoms also diffused into the oxidation layer, promoting the injection of electrons into the ZnS NRs *via* direct tunneling due to the increase of the interfacial doping concentration and the decrease of the barrier width of the interface (Fig. 3c).[25] The interfacial oxide layer should have a composition similar to that of ZnInO (IZO), which is a material usually used in transparent oxide electrodes. The surface reaction is further enhanced by the post-annealing process, thus leading to the improvement of the conductivity. The achievement of good ohmic contact by using ITO would become the critical step in the practical application of ZnS nanostructures in nano-electronics and nano-optoelectronics. In addition, the use of transparent ITO electrodes would facilitate the design and implementation of fully transparent ZnS nanodevices.

3.3 Electrical transport properties of the ZnS:Cl NRs

The electrical transport characteristics of the ZnS:Cl NR FETs are shown in Fig. 4. From the typical source–drain current (I_{DS}) *versus* source–drain voltage (V_{DS}) curves measured at varied V_G, it is clear that all the devices show an obvious gating effect and the conductance of ZnS:Cl NRs increases with the increasing of V_G, which is consistent with the typical characteristics of an n-channel metal-oxide-semiconductor FET (MOSFET) and thus reveals the n-type nature of the Cl doped ZnS NRs. Table 1 summarizes the key parameters of the nano-FETs that are fabricated from the ZnS:Cl NRs with varied doping levels, in which the threshold value (V_{th}) is deduced by extracting the linear portion of the I_{DS}–V_G plot, and the electron mobility (μ_n) can be estimated from the channel transconductance (g_m) of the nano-FETs according to the equation $g_m = \partial I_{DS}/\partial V_G = Z\mu_n C_0 V_{DS}/L$ in the linear regime of I_{DS}–V_G curves, where Z/L is the width-to-length ratio of the NR channel, and C_0 is the oxide capacitance per unit area. I_{ON}/I_{OFF} ratio is estimated from the I_{DS} at the ON state (+40 V) and OFF state (−30 V) and the electron concentration (n) is calculated from the equation $n = \sigma/q\mu_n$, where σ is the conductivity of the NRs at $V_G = 0$ V. From Table 1, it is noticed that V_{th} has gradually decreased from sample 1 to 3, which is due to the increasing of carrier concentration from sample 1 to 3 and consequently lower voltage is needed to turn-on the devices. Both g_m and μ_n are enhanced with increasing doping level and a mobility value as high as 82.1 $cm^2 V^{-1} s^{-1}$ is estimated for sample 3, which might be attributed to the higher channel conduction and improved electrical contact at high doping level.[26] Significantly, n increases remarkably with the increasing of Cl doping level and the highest electron concentration (3.8×10^{17} cm^{-3}) is obtained for sample 3. This value is comparable with that achieved from ZnS:Cl films.[27] On the other hand, the modulation of gate voltage to the channel conduction becomes weaker when n is increased. As a result, the I_{ON}/I_{OFF} ratio decreases from $\sim 10^5$ for sample 1 to a small value of ~ 10 for sample 3. Results reported here undoubtedly demonstrate that the electrical properties of n-ZnS NRs could be effectively tuned by varying the Cl doping concentration.

3.4 High-gain visible-blind UV photodetectors based on the ZnS:Cl NRs

The ZnS:Cl NRs show promising application as high-performance visible-light blind UV nano-photodetectors. Fig. 5a plots the I–V curves of an individual ZnS:Cl NR (from sample 1)

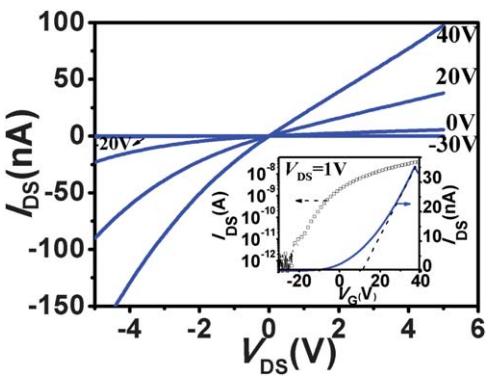

Fig. 4 Electrical transfer characteristics of ZnS:Cl NRs from sample 1. I_{DS}–V_{DS} curves plotted at varied V_G. Inset shows the I_{DS}–V_G curves at $V_{DS} = 1$ V.

Table 1 Summary of the key device parameters of the ZnS:Cl NR FETs

	V_{th} (V)	I_{ON}/I_{OFF}	g_m (nS)	μ_n (cm^2 V^{-1} s^{-1})	n ($\times 10^{17}$ cm^{-3})
Sample 1	10.3	$\sim 10^5$	1.3	2.8	0.16
Sample 2	−6.1	$\sim 10^3$	4.6	10.0	1.6
Sample 3	−40	$\sim 10^1$	57.5	82.1	3.8

under the light illumination with varied wavelength. The conductance of the ZnS:Cl NRs strongly depends on the light wavelength and the photocurrent increases remarkably in the short wavelength range but is nearly constant (equal to the dark current) in the visible range. Fig. 5b depicts the spectral dependence of the sensitivity. The cut-off wavelength of ~330 nm is consistent with the bandgap of ZnS, revealing that the increase of the photocurrent is mainly due to the electron–hole pairs excited by the incident light with energy greater than the bandgap. From the time response spectra of the ZnS:Cl NRs (Fig. 5c) it is observed that the nano-photodetectors exhibit excellent stability and reproducibility, and the doping concentration has significant influence on the photoconductive characteristics of the ZnS:Cl NRs. Rise time (t_r) and fall time (t_f) of sample 1 are 46 s and 30 s, respectively. As for sample 3, t_r increases slightly to 76 s, while t_f increases significantly to 463 s. At the same time, the I_{light}/I_{dark} ratio decreases from $\sim 10^3$ for sample 1 to $\sim 10^1$ for sample 3. The decrease of the I_{light}/I_{dark} ratio can be attributed to the large dark current at the high doping level, while the increase of response time is associated with the defects in the ZnS:Cl NRs. The carrier trap centers caused by the Cl doping trap the photo-generated carriers during the UV illumination and gradually release them after the light is off, leading to a long decay edge. Therefore, the high concentration of trap centers in sample 3 could account for the low response speed. However, we note the response speed of the ZnS:Cl NRs is comparable with that of the ZnO and GaN UV nano-photodetectors in previous reports.[13,14,28]

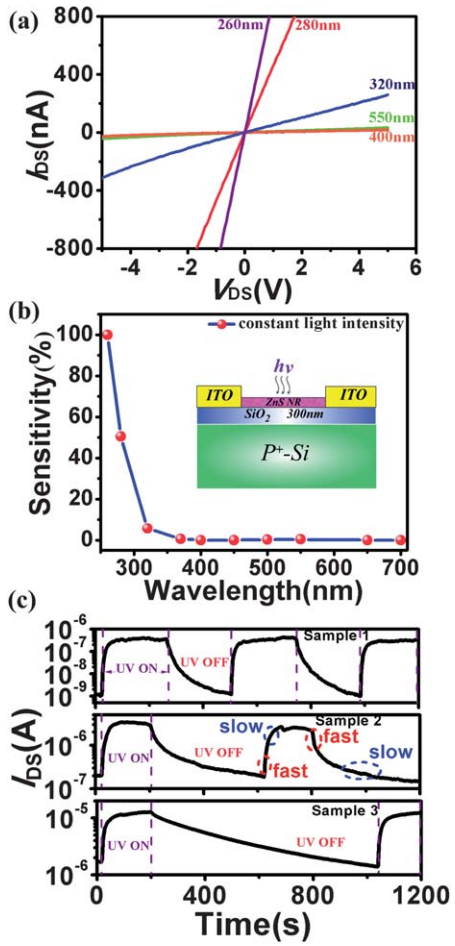

Fig. 5 (a) *I–V* curves of a single ZnS:Cl NR (sample 1) illuminated by the light with different wavelength from 260 nm to 650 nm at a constant light intensity of 100 μW cm^{-2}. (b) Spectral response of the ZnS:Cl NR (sample 1). The inset shows the schematic diagram for the photoconductive measurement. (c) Time response of the ZnS:Cl NRs to the pulsed UV-light (254 nm, 300 μW cm^{-2}). V_{DS} is fixed at 1 V.

Responsivity (R) is an important factor which reflects the electrical output per optical input of a photodetector. A higher responsivity is desired in order to achieve higher response for a given incidence light. R is defined as

$$R\ (\mathrm{A\ W^{-1}}) = \frac{I_p}{P_{opt}} = \eta\left(\frac{q\lambda}{hc}\right)G$$

where I_p, P_{opt}, η, λ, h, c and G are photocurrent, incident light power, quantum efficiency, light wavelength, Planck's constant, and photoconductive gain, respectively. Based on the equation, R is estimated to be 9.7×10^4 A W^{-1} for sample 1 at $V_{DS} = 1$ V by assuming $\eta = 1$ for simplification, and a maximum value of 2.9×10^6 A W^{-1} is obtained for sample 3. Meanwhile, G increases from 4.8×10^5 for sample 1 to 1.4×10^7 for sample 3. Such a result suggests that a large internal gain exists in the ZnS:Cl NR photodetectors. For comparison, R and G values for various UV nano-photodetectors are shown in Table 2. Significantly, R and G in this work represent one of the best values obtained for the UV nano-photodetectors, which are at least five orders of magnitude higher than the previous report on an intrinsic ZnS NR photodetector,[15] and are comparable with the best values obtained for ZnO and GaN nano-photodetectors. Such a high gain could even allow reaching single-photon detectivity in single NRs.[13] Although a slow photocurrent relaxation time is observed

Table 2 Summary of the photoconductive properties of the ZnS:Cl NRs. Values from previous reports are also presented for comparison

	t_r (s)	t_f (s)	I_{light}/I_{dark}	R_{max} (A W^{-1})	G_{max}
Sample 1	46	30	$\sim 10^3$	9.7×10^4	4.8×10^5
Sample 2	59	86	$\sim 10^2$	8.2×10^5	4.0×10^6
Sample 3	76	463	$\sim 10^1$	2.9×10^6	1.4×10^7
*ZnS NR*15	~3	~3	$\sim 10^1$	~0.2	
*ZnO NR*28		~400	$\sim 10^3$	$\sim 10^2$	$\sim 10^2$
*ZnO NW*13	~40	~120	$\sim 10^4$		$\sim 10^8$
*GaN NW*14		~300	$\sim 10^1$	$\sim 10^2$	$\sim 10^2$ 29

for the ZnS:Cl NRs, the high gain values can result in a large gain-bandwith. Therefore, a significant photoresponse is excepted for the NR photodetector and they are expected to work at high modulation frequencies. [13] The substantial improvement in the responsivity and photoconductive gain can be attributed to the presence of deep level trap states in ZnS:Cl NRs. The trap states caused by Cl doping can trap the minority carriers (holes), leading to a great prolongation of the lifetime of the photocarriers (electrons) by preventing electron–hole recombination.[13,30] In contrast, in the undoped ZnS NRs, recombination will happen as soon as the electron–hole pairs are generated by the excitation light. Only a small amount of carriers can reach the electrodes and thus contribute little to the photocurrent.

To further assess the capability of the Cl-doped ZnS NRs as high-speed photodetectors, a pulsed UV light that was generated by a frequency-tunable mechanical chopper was used to irradiate the NR, as shown in Fig. 6a. Interestingly, it was found that the NR can follow the pulsed light well up to 100 Hz; at that frequency the $(I_{max} - I_{min})/I_{max}$ ratio is still close to 20% (Fig. 6b). At first glance, this result has conflicted with the above measurements (Fig. 5c), where a much longer rise and fall time are observed. Nevertheless, closer investigation of Fig. 5c reveals that both the rise and the fall edges of the samples are composed of two response components, *i.e.*, the fast component corresponding to the direct electron–hole generation (for rise edges) and recombination (for fall edges), whereas the slow component is caused by the carriers filling (for rise edges) and releasing (for fall edges) due to the presence of the trapper centers. By utilizing the fast response component only instead of the full rise (fall) edges, a fast response to the incident UV light is achieved. Although the maximum photocurrent will inevitably decrease with an increase in the light frequency, the large responsivity of the ZnS:Cl NRs still allows a significant response to pulsed UV light.

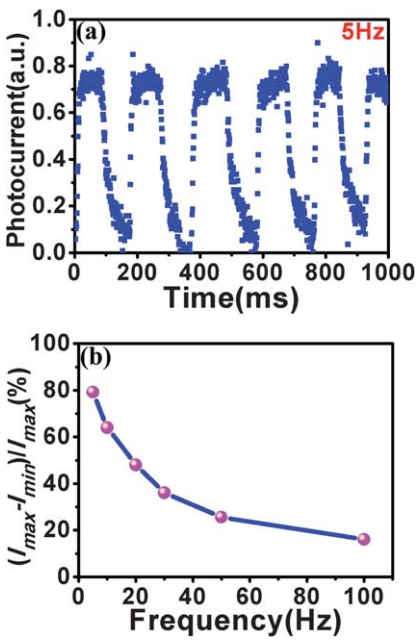

Fig. 6 (a) Response characteristics of the ZnS:Cl NRs (sample 1) to the pulsed UV light (320 nm, 300 μW cm^{-2}) at a frequency of 5 Hz. (b) The relative balance $(I_{max} - I_{min})/I_{max}$ *versus* switching frequency.

4 Conclusion

In conclusion, we have demonstrated the tuning of electronic and optoelectronic properties of n-type ZnS NRs by chloride doping *via* a simple thermal co-evaporation method. Ohmic contact was successfully achieved by using ITO instead of conventional metallic electrodes. By adjusting the Cl dopant level, the conductivity of the n-type ZnS:Cl NRs could be tuned in a wide range of 3–4 orders of magnitude. In addition, nano-photodetectors constructed from the ZnS:Cl NRs exhibit excellent device performance with extremely high sensitivity to the UV light while are nearly blind to the visible light. The photoconductive gain of the ZnS:Cl NR photodetectors is as high as 10^7. The value is among the highest values obtained for nanostructure-based UV photodetectors so far. Fast response to the pulsed UV light with frequency up to 100 Hz was also observed for the devices. It is expected that n-type ZnS NRs with tunable optoelectronic properties will have important applications in the nano-electronics and nano-optoelectronic devices.

Acknowledgements

This work was supported by the National Natural Science Foundation of China (Nos. 60806028, 20901021, 50903059), the Program for New Century Excellent Talents in the University of the Chinese Ministry of Education (NCET-08-0764), the Major Research Plan of the National Natural Science Foundation of China (No. 91027021), the Fundamental Research Funds for the Central Universities, the Foundation of Hefei University of Technology (2009HGXJ0015), the Natural Science Foundation of the Jiangsu Higher Education Institutions of China (Grant No. 09KJB430009), and the Specialized Research Fund for the Doctoral Program of Higher Education of China (Grant No. 20093201120020).

Notes and references

1 M. Bredol and J. Merikhi, *J. Mater. Sci.*, 1998, **33**, 471.
2 L. D. Sun, C. H. Liu, C. S. Liao and C. H. Yan, *J. Mater. Chem.*, 1999, **9**, 1655.
3 T. Yamamoto, S. Kishimoto and S. Iida, *Phys. B*, 2001, **308**, 916.
4 J. A. Zapien, Y. Jiang, X. M. Meng, W. Chen, F. C. K. Au, Y. Lifshitz and S. T. Lee, *Appl. Phys. Lett.*, 2004, **84**, 1189.
5 A. Datta, S. K. Panda and S. Chaudhuri, *J. Solid State Chem.*, 2008, **181**, 2332.
6 B. Y. Geng, L. D. Zhang, G. Z. Wang, T. Xie, Y. G. Zhang and G. W. Meng, *Appl. Phys. Lett.*, 2004, **84**, 2157.
7 T. Kang, J. Sung, W. Shim, H. Moon, J. Cho, Y. Jo, W. Lee and B. Kim, *J. Phys. Chem. C*, 2009, **113**, 5352.
8 S. L. Hou, Y. Y. Yuen, H. B. Mao, J. Q. Wang and Z. Q. Zhu, *J. Phys. D: Appl. Phys.*, 2009, **42**, 215105.
9 M. Y. Lu, L. J. Chen, W. J. Mai and Z. L. Wang, *Appl. Phys. Lett.*, 2008, **93**, 242503.
10 B. C. Cheng and Z. G. Wang, *Adv. Funct. Mater.*, 2005, **15**, 1883.
11 G. D. Yuan, W. J. Zhang, W. F. Zhang, X. Fan, I. Bello, C. S. Lee and S. T. Lee, *Appl. Phys. Lett.*, 2008, **93**, 213102.
12 M. Y. Lu, M. P. Lu, Y. A. Chung, M. J. Chen, Z. L. Wang and L. J. Chen, *J. Phys. Chem. C*, 2009, **113**, 12878.
13 C. Soci, A. Zhang, B. Xiang, S. A. Dayeh, D. P. R. Aplin, J. Park, X. Y. Bao, Y. H. Lo and D. Wang, *Nano Lett.*, 2007, **7**, 1003.
14 R. Calarco, M. Marso, T. Richter, A. I. Aykanat, R. Meijers, A. v. d. Hart, T. Stoica and H. Lüth, *Nano Lett.*, 2005, **5**, 981.
15 X. S. Fang, Y. S. Bando, M. Y. Liao, U. K. Gautam, C. Y. Zhi, B. Dierre, B. D. Liu, T. Y. Zhai, T. Sekiguchi, Y. Koide and D. Golberg, *Adv. Mater.*, 2009, **21**, 2034–2039.

16 X. S. Fang, Y. Bando, M. Y. Liao, T. Y. Zhai, U. K. Gautam, L. Li, Y. Koide and D. Golberg, *Adv. Funct. Mater.*, 2010, **20**, 500.
17 A. Kato, M. Katayama, A. Mizutani, Y. Hattori, N. Ito and T. Hattori, *J. Appl. Phys.*, 1994, **76**, 3206.
18 H. Luo and J. K. Furdyna, *Semicond. Sci. Technol.*, 1995, **10**, 1041.
19 P. Prathap, N. Revathi, Y. P. V. Subbaiah, K. T. Ramakrishna Reddy and R. W. Miles, *Solid State Sci.*, 2009, **11**, 224.
20 K. Era, S. Shionoya, Y. Washizawa and H. Ohmatsu, *J. Phys. Chem. Solids*, 1968, **29**, 1843.
21 S. X. Zhou, Y. G. Wang, W. Han and N. Wang, *J. Phys. Chem. C*, 2008, **112**, 18644.
22 J. H. He, Y. Y. Zhang, J. Liu, D. Moore, G. Bao and Z. L. Wang, *J. Phys. Chem. C*, 2007, **111**, 12152.
23 S. M. Sze. *Physics of Semiconductor Devices*, Wiley: New York, 1981.
24 R. K. Swank, *Phys. Rev.*, 1967, **153**, 844.
25 G. X. Hu, B. Kumar, H. Gong, E. F. Chor and P. Wu, *Appl. Phys. Lett.*, 2006, **88**, 101901.
26 G. F. Zheng, W. Lu, S. Jin and C. M. Lieber, *Adv. Mater.*, 2004, **16**, 1890.
27 J. W. Cook, Jr., D. B. Eason, R. P. Vaudo and J. F. Schetzina, *J. Vac. Sci. Technol., B*, 1992, **10**, 901.
28 Y. K. Su, S. M. Peng, L. W. Ji, C. Z. Wu, W. B. Cheng and C. H. Liu, *Langmuir*, 2010, **26**, 603.
29 R. S. Chen, H. Y. Chen, C. Y. Lu, K. H. Chen, C. P. Chen, L. C. Chen and Y. J. Yang, *Appl. Phys. Lett.*, 2007, **91**, 223106.
30 B. W. Lim, Q. C. Chen, J. Y. Yang and M. A. Khan, *Appl. Phys. Lett.*, 1996, **68**, 3761.

